Charge Penetration and the Origin of Large O−H Vibrational Red-Shifts in Hydrated-Electron Clusters, $(H_2O)_n^-$

John M. Herbert*,† and Martin Head-Gordon

Contribution from the Department of Chemistry, University of California, Berkeley, California 94720

Received July 12, 2006; E-mail: herbert@chemistry.ohio-state.edu

Abstract: The origin of O−H vibrational red-shifts observed experimentally in $(H_2O)_n^-$ clusters is analyzed using electronic structure calculations, including natural bond orbital analysis. The red-shifts are shown to arise from significant charge transfer and strong donor−acceptor stabilization between the unpaired electron and O−H σ^* orbitals on a nearby water molecule in a double hydrogen-bond-acceptor ("AA") configuration. The extent of $e^- \rightarrow \sigma^*$ charge transfer is comparable to the $n \rightarrow \sigma^*$ charge transfer in the most strongly hydrogen-bonded $X^-(H_2O)$ complexes (e.g., X = F, O, OH), even though the latter systems exhibit much larger vibrational red-shifts. In $X^-(H_2O)$, the proton affinity of X^- induces a low-energy $XH\cdots^-OH$ diabatic state that becomes accessible in $v = 1$ of the shared-proton stretch, leading to substantial anharmonicity in this mode. In contrast, the $H + {}^-OH(H_2O)_{n-1}$ diabat of $(H_2O)_n^-$ is not energetically accessible; thus, the O−H stretching modes of the AA water are reasonably harmonic, and their red-shifts are less dramatic. Only a small amount of charge penetrates beyond the AA water molecule, even upon vibrational excitation of these AA modes. Implications for modeling of the aqueous electron are discussed.

Introduction

Infrared spectra obtained for individual isomers of size-selected $(H_2O)_n^-$ cluster anions[1−5] exhibit very intense O−H stretching transitions that are red-shifted by about 300 cm^{-1} relative to isolated H_2O. On the basis of electronic structure calculations[2−4] these red-shifted features are assigned to stretching and bending vibrations localized on a water molecule in a double hydrogen-bond-acceptor ("AA") configuration. This water molecule has two "dangling" hydrogen atoms that are not involved in hydrogen bonds to other water molecules, and these serve to solvate the excess electron. In small clusters, the singly occupied molecular orbital (SOMO), which identifies the electron binding motif, remains localized near these two hydrogen atoms, even in the presence of thermal fluctuations at $T = 300$ K.[6] Although the experimental vibrational spectra for size-selected $(H_2O)_n^-$ clusters have so far been definitively assigned to particular cluster isomers only for $n \leq 6$, the intense, strongly red-shifted features persist in larger clusters. Spectra up to $n = 24$ have been reported[5,7] and appear to exhibit the same features (albeit considerably broadened) that for $n = 3-6$ are indicative of the AA electron binding motif. The persistence of this binding motif is interesting in view of resonance Raman spectra of the bulk aqueous electron that appear to rule out the AA binding motif in the bulk.[8]

The precise origin of the vibrational red-shifts has remained a mystery. Clusters as small as $(H_2O)_3^-$ exhibit the shift but possess vertical electron binding energies (VEBEs) so small that these anions are usually considered to be dipole-bound,[9,10] terminology suggestive of a SOMO that remains localized at the positive end of the cluster dipole moment and does not penetrate into the water network. On the other hand, there is much precedent for large vibrational red-shifts arising from anion−water hydrogen bonds (H-bonds). Halide−water clusters, in particular, have been studied extensively by vibrational spectroscopy,[11−19] and the spectra of small clusters are well

† Present address: Department of Chemistry, The Ohio State University, Columbus, OH 43210.

(1) Ayotte, P.; Bailey, C. G.; Kim, J.; Johnson, M. A. *J. Chem. Phys.* **1998**, *108*, 444.
(2) Hammer, N. I.; Shin, J.-W.; Headrick, J. M.; Diken, E. G.; Roscioli, J. R.; Weddle, G. H.; Johnson, M. A. *Science* **2004**, *306*, 675.
(3) Hammer, N. I.; Roscioli, J. R.; Johnson, M. A. *J. Phys. Chem. A* **2005**, *109*, 7896.
(4) Hammer, N. I.; Roscioli, J. R.; Johnson, M. A.; Myshakin, E. M.; Jordan, K. D. *J. Phys. Chem. A* **2006**, *109*, 11526.
(5) Roscioli, J. R.; Hammer, N. I.; Johnson, M. A. *J. Phys. Chem. A* **2006**, *110*, 7517.
(6) Herbert, J. M.; Head-Gordon, M. *Proc. Natl. Acad. Sci. U.S.A.* **2006**, *103*, 14282.
(7) Hammer, N. I.; Roscioli, J. R.; Bopp, J. C.; Headrick, J. M.; Johnson, M. A. *J. Chem. Phys.* **2005**, *123*, 244311.

(8) Tauber, M. J.; Mathies, R. A. *J. Am. Chem. Soc.* **2003**, *125*, 1394.
(9) Gutowski, M.; Jordan, K. D.; Skurski, P. *J. Phys. Chem. A* **1998**, *102*, 2624.
(10) Jordan, K. D.; Wang, F. *Annu. Rev. Phys. Chem.* **2003**, *54*, 367.
(11) Ayotte, P.; Weddle, G. H.; Kim, J.; Johnson, M. A. *Chem. Phys.* **1998**, *239*, 485.
(12) Ayotte, P.; Weddle, G. H.; Kim, J.; Johnson, M. A. *J. Am. Chem. Soc.* **1998**, *120*, 12361.
(13) Ayotte, P.; Bailey, C. G.; Weddle, G. H.; Johnson, M. A. *J. Phys. Chem. A* **1998**, *102*, 3067.
(14) Ayotte, P.; Nielsen, S. B.; Weddle, G. H.; Johnson, M. A.; Xantheas, S. S. *J. Phys. Chem. A* **1999**, *103*, 10665.
(15) Choi, J.-H.; Kuwata, K. T.; Cao, Y.-B.; Okumura, M. *J. Phys. Chem. A* **1998**, *102*, 503.
(16) Robertson, W. H.; Johnson, M. A. *Annu. Rev. Phys. Chem.* **2003**, *54*, 173.
(17) Cabarcos, O. M.; Weinheimer, C. J.; Lisy, J. M.; Xantheas, S. S. *J. Chem. Phys.* **1999**, *110*, 5.
(18) Diken, E. G.; Headrick, J. M.; Roscioli, J. R.; Bopp, J. C.; Johnson, M. A.; McCoy, A. B.; Huang, X.; Bowman, J. M. *J. Phys. Chem. A* **2005**, *109*, 571.
(19) Roscioli, J. R.; Diken, E. G.; Johnson, M. A.; Horvath, S.; McCoy, A. B. *J. Phys. Chem. A* **2006**, *110*, 4943.

understood on the basis of theoretical predictions and assignments.[17−32] Vibrational red-shifts arising from H-bonds to the anion often greatly exceed the 300 cm^{-1} observed for hydrated-electron clusters; for example, the two O−H stretching vibrations in F^{-}(H$_2$O) are split by over 2100 cm^{-1} (ref 19). That said, it is not clear that e^{-} is a typical anion, though we will demonstrate that charge transfer into antibonding orbitals of the water molecules is just as significant in certain isomers of (H$_2$O)$_n^{-}$ as it is in strongly H-bonded complexes such as F^{-}(H$_2$O).

In this work we utilize electronic structure theory—including natural bond orbital (NBO) calculations[33,34] as well as a detailed analysis of vibrational spectra for several isomers of (H$_2$O)$_4^{-}$, (H$_2$O)$_6^{-}$, and the corresponding neutral clusters—to demonstrate that vibrational red-shifts in small (H$_2$O)$_n^{-}$ clusters arise primarily as a result of substantial charge transfer and strong donor−acceptor stabilization between the unpaired electron and O−H σ^* antibonding orbitals on a nearby AA water molecule. There is little charge transfer beyond the AA water molecule, and non-AA isomers exhibit substantially less charge penetration. In contrast to $n \rightarrow \sigma^*$ charge transfer in other anion−water clusters, which is enhanced by electron correlation but present even in a mean-field treatment, $e^{-} \rightarrow \sigma^*$ charge transfer in (H$_2$O)$_n^{-}$ is almost entirely an electron correlation effect. This observation may have important implications for the design of electron−water pseudopotentials for mixed quantum/classical simulations of the aqueous electron.

Computational Methods

For most details regarding basis sets, thresholds, and the performance of various electronic structure models, the reader is referred to our previous work.[6,35,36] Briefly, we calculate harmonic frequencies using the B3LYP density functional[37,38] and the aug3-cc-pVDZ basis set[35] (a triply augmented version of aug-cc-pVDZ) and then scale these frequencies and convolve them with 8 cm^{-1} Lorentzians (full width at half-maximum) in order to obtain vibrational spectra. The scale factor for the bend region is chosen to reproduce the bending frequency of H$_2$O, and that for the stretching region is chosen to reproduce the average of the two stretching frequencies in H$_2$O. This procedure has been shown to reproduce experimental frequencies and intensities in small (H$_2$O)$_n^{-}$ clusters.[2−4,6]

NBO calculations for X^{-}(H$_2$O) employ the 6-31++G* basis (although the results are stable with respect to basis-set expansion). The NBO algorithm behaves somewhat erratically when highly diffuse basis functions are present, so NBO calculations on (H$_2$O)$_n^{-}$ utilize the 6-31++G* basis in conjunction with a ghost atom that supports two sets of sp functions with orbital exponents of 0.020 and 0.005 bohr, comparable to the most diffuse hydrogen s functions in aug3-cc-pVDZ. Following previous notation,[35] we denote this composite basis as 6-31++G*-f(2+), where "f" stands for "floating center". Initially, the ghost atom is placed at the centroid of the SOMO (as determined from a prior calculation using only atom-centered basis functions), and subsequently the cluster geometry (including the ghost atom) is re-optimized using the new basis set. Ghost-atom basis functions were selected, after some experimentation, because B3LYP/6-31++G*-f(2+) vibrational spectra and SOMO radii of gyration are in qualitative agreement with B3LYP/aug3-c-pVDZ results, and coupled-cluster VEBEs calculated with the ghost-atom basis are also in reasonable agreement with accurate values. Vibrational frequencies in the ghost-atom basis are calculated by setting the mass of the ghost atom to 10,000 amu, effectively decoupling this atom from the real vibrational modes. All NBO calculations employ B3LYP geometries.

NBO calculations at the second-order Møller−Plesset (MP2) level utilize the MP2 relaxed density matrix from an MP2 gradient calculation. Where necessary, small adjustments ($\lesssim 0.05$) are made to the eigenvalues of this matrix so that all eigenvalues are contained in the interval [0,1] and sum to the number of electrons.

All calculations are performed using Q-Chem,[39] which includes v. 5.0 of the NBO program of Weinhold and co-workers.[40] Orbital plots are rendered using Visual Molecular Dynamics.[41]

Results and Discussion

Comparative NBO Analysis of X^{-}(H$_2$O) and (H$_2$O)$_n^{-}$. We begin not with (H$_2$O)$_n^{-}$ but with traditional anion monohydrates X^{-}(H$_2$O), whose vibrational spectra exhibit strong red-shifts of the shared-proton stretch.[12,18,19] Previous calculations[19,20] have established that the minimum-energy structures of these complexes exhibit only one anion−water H-bond (C_s rather than C_{2v} symmetry). The charge-transfer character of halide−water complexes has been investigated previously using Löwdin population analysis,[25,42] but we revisit these systems with NBO analysis in order to make subsequent comparison to (H$_2$O)$_n^{-}$.

NBO analysis of various X^{-}(H$_2$O) complexes at the Hartree−Fock (HF), MP2, and B3LYP levels of theory is summarized in Table 1. When the anion is a strong base (X = F, O, and OH), there is significant occupancy in the σ_{OH}^* orbital of the H-bonded O−H moiety, up to 0.16 electrons. Most of this occupancy is present in the uncorrelated HF calculation, though correlation enhances the σ_{OH}^* occupancy by 0.02−0.03 electrons. The trend in σ_{OH}^* occupancies mirrors the trend in O−H vibrational red-shifts, with the mostly charge-localized Cl^{-}(H$_2$O) system exhibiting a σ_{OH}^* occupancy of 0.05 electrons and a red-shift of 570 cm^{-1}, compared to 0.11 electrons and 2100 cm^{-1} for F^{-}(H$_2$O).

The origin of the σ_{OH}^* occupancies may be ascertained by analyzing donor−acceptor stabilization energies (hyperconju-

(20) Yates, B. F.; Schaefer, H. F., III; Lee, T. J.; Rice, J. E. *J. Am. Chem. Soc.* **1988**, *110*, 6327.
(21) Xantheas, S. S. *J. Phys. Chem.* **1996**, *100*, 9703.
(22) Dorsett, H. E.; Watts, R. O.; Xantheas, S. S. *J. Phys. Chem. A* **1999**, *103*, 3351.
(23) Satoh, K.; Iwata, S. *Chem. Phys. Lett.* **1999**, *312*, 522.
(24) Schenter, G. K.; Garrett, B. C.; Voth, G. A. *J. Chem. Phys.* **2000**, *113*, 5171.
(25) Kim, J.; Lee, H. M.; Suh, S. B.; Majumdar, D.; Kim, K. S. *J. Chem. Phys.* **2000**, *113*, 5259.
(26) Lee, H. M.; Kim, D.; Kim, K. S. *J. Chem. Phys.* **2002**, *116*, 5509.
(27) Masamura, M. *J. Chem. Phys.* **2003**, *118*, 6336.
(28) Chaban, G. M.; Jung, J. O.; Gerber, R. B. *J. Chem. Phys.* **1999**, *111*, 1823.
(29) Chaban, G. M.; Xantheas, S. S.; Gerber, R. B. *J. Phys. Chem. A* **2003**, *107*, 4952.
(30) Irle, S.; Bowman, J. M. *J. Chem. Phys.* **2000**, *113*, 8401.
(31) Bowman, J. M.; Xantheas, S. S. *Pure Appl. Chem.* **2004**, *76*, 29.
(32) Rheinecker, J. L.; Bowman, J. M. *J. Chem. Phys.* **2006**, *124*, 131102.
(33) Reed, A. E.; Curtiss, L. A.; Weinhold, F. *Chem. Rev.* **1988**, *88*, 899.
(34) Weinhold, F. Natural bond orbital methods; In *Encyclopedia of Computational Chemistry*; Schleyer, P. v. R., Allinger, N. L., Clark, T., Gasteiger, J., Kollman, P. A.. Schaefer, H. F., III, Schreiner, P. R., Eds.; Wiley: Chichester, United Kingdom, 1999; Vol. 3, p 1792.
(35) Herbert, J. M.; Head-Gordon, M. *J. Phys. Chem. A* **2005**, *109*, 5217.
(36) Herbert, J. M.; Head-Gordon, M. *Phys. Chem. Chem. Phys.* **2006**, *8*, 68.
(37) Becke, A. D. *J. Chem. Phys.* **1993**, *98*, 5648.
(38) Stephens, P. J.; Devlin, J. F.; Chabalowski, C. F.; Frisch, M. J. *J. Phys. Chem.* **1994**, *98*, 11623.

(39) Shao, Y.; et al. *Phys. Chem. Chem. Phys.* **2006**, *8*, 3172.
(40) Glendening, E. D.; Badenhoop, J. K.; Reed, A. E.; Carpenter, J. E.; Bohmann, J. A.; Morales, C. M.; Weinhold, F. *NBO*, 5.0, Technical report; Theoretical Chemistry Institute, University of Wisconsin: Madison, WI, 2001.
(41) Humphrey, W.; Dalke, A.; Schulten, K. *J. Mol. Graphics* **1996**, *14*, 33.
(42) Combariza, J. E.; Kestner, N. R.; Jortner, J. *J. Chem. Phys.* **1994**, *100*, 2851.

Table 1. NBO Occupancies and Donor–Acceptor (D → A) Stabilization Energies for X$^-$(H$_2$O) Complexes

		HF[a]			MP2[a]			B3LYP[a]		
		occup.[b]		$\Delta E_{D \to A}$	occup.[b]		$\Delta E_{D \to A}$	occup.[b]		$\Delta E_{D \to A}$
complex	D → A interaction	D	A	(kcal/mol)[c]	D	A	(kcal/mol)[c]	D	A	(kcal/mol)[c]
HO$^-$ (H$_2$O)	n(O) → σ*(OH)	1.86	0.13	112.9	1.82	0.17	111.9	1.83	0.16	87.2
	n'(O) → σ*(OH)	2.00	0.13	4.2	1.97	0.17	7.0	2.00	0.16	4.7
O$^-$(H$_2$O)	n(O) → σ*(OH)	1.86	0.14	106.7	1.82	0.16	105.0	1.83	0.16	81.0
	n'(O) → σ*(OH)	2.00	0.14	5.6	1.98	0.16	7.7	2.00	0.16	5.3
F$^-$(H$_2$O)	n(F) → σ*(OH)	1.91	0.09	80.1	1.87	0.12	77.6	1.88	0.11	64.4
	n'(F) → σ*(OH)	2.00	0.09	5.4	1.98	0.12	8.5	2.00	0.11	5.6
Cl$^-$(H$_2$O)	n(Cl) → σ*(OH)	1.96	0.04	20.5	1.93	0.06	19.8	1.94	0.05	17.0

[a] 6-31++G* basis at the B3LYP/6-31++G* geometry. [b] Sum of α and β occupancies. [c] All stabilization energies larger than 4.0 kcal/mol per electron pair are listed.
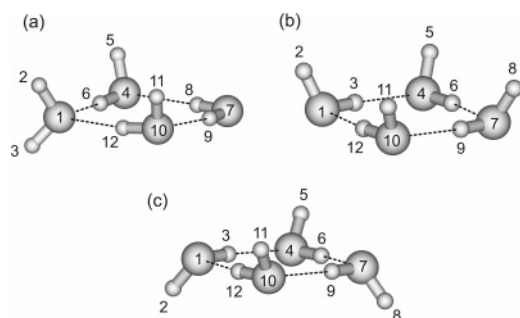

Figure 1. Isomers of (H$_2$O)$_4$ and (H$_2$O)$_4^-$ considered in this work: (a) an AA-type isomer of (H$_2$O)$_4^-$, (b) a cyclic isomer of (H$_2$O)$_4^-$, and (c) the most stable isomer of (H$_2$O)$_4$.
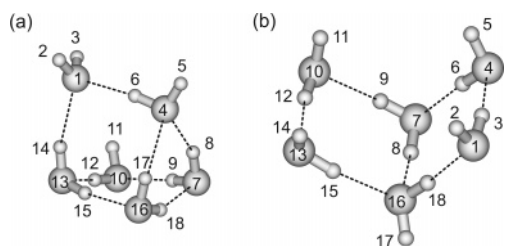
Figure 2. Isomers of (H$_2$O)$_6^-$ considered in this work: (a) an AA-type isomer of (H$_2$O)$_6^-$ and (b) a "book" isomer of (H$_2$O)$_6^-$. The book isomer of (H$_2$O)$_6$ considered here is almost identical to the structure shown in (b).

gation energies) between NBOs. If ϕ_D and ϕ_A are NBOs, then the $\phi_D \to \phi_A$ stabilization energy is estimated from second-order perturbation theory according to[34]

$$\Delta E_{D \to A} = -p_D \frac{|\langle \phi_D | \hat{F} | \phi_A \rangle|^2}{\epsilon_A - \epsilon_D}$$

where $\hat{F}$ is the Fock operator, p_D is the occupancy of ϕ_D, and $\epsilon_i = \langle \phi_i | \hat{F} | \phi_i \rangle$. The numerical values of these stabilization energies can be quite large on a chemical scale (e.g., 10−100 kcal/mol for a strong hydrogen bond), and we will not attempt to assign any chemical significance or interpretation to these absolute numbers. Their utility lies in the comparison of different donor–acceptor stabilization energies. For X$^-$(H$_2$O), the only significant stabilization energies are those associated with $n \to \sigma_{OH}^*$ charge transfer (see Table 1), and this unambiguously identifies $n \to \sigma_{OH}^*$ charge transfer as the origin of the rather significant σ_{OH}^* populations.

The foregoing analysis establishes a backdrop against which to compare the representative (H$_2$O)$_n$ isomers shown in Figures 1 and 2. These include AA isomers of (H$_2$O)$_4^-$ and (H$_2$O)$_6^-$ [Figures 1a and 2a], a cyclic isomer of (H$_2$O)$_4^-$ [Figure

1b, which is the lowest-energy (H$_2$O)$_4^-$ isomer yet identified[6]] and a "book" isomer of (H$_2$O)$_6^-$ [Figure 2b]. Each of these has been assigned to a peak in the (H$_2$O)$_4^-$ or (H$_2$O)$_6^-$ photoelectron spectrum,[3,43] and vibrational spectra have been measured[2,3] for each, save for cyclic (H$_2$O)$_4^-$. As points of comparison, we also consider a cyclic isomer of (H$_2$O)$_4$ [Figure 1c, which is the global minimum for the neutral tetramer,[44,45]] and also a book isomer of (H$_2$O)$_6$ similar to the structure in Figure 2b.

For the AA isomers of both (H$_2$O)$_4^-$ and (H$_2$O)$_6^-$, NBO analysis affords five α-spin NBOs associated with the unpaired electron, whose occupancies range from 0.10 to 0.36 at the B3LYP level. These are depicted for (H$_2$O)$_6^-$ in Figure 3, while those for AA (H$_2$O)$_4^-$ are quite similar. All other NBOs have occupancies less than 0.05 or greater than 0.98. Taken together, the five excess-electron NBOs account for 0.90 electrons in the case of (H$_2$O)$_4^-$ and 0.84 electrons in the case of (H$_2$O)$_6^-$; thus, although the unpaired electron cannot be associated with a *single* NBO (because it is not associated with a single atom), an excellent description can be obtained with a near-minimal basis of NBOs.

The nature of the excess-electron NBOs in the AA-type isomers is easily understood. First, there is a single-center Rydberg-type (Ry) NBO associated with each hydrogen of the AA water, as depicted in Figure 3a,b. These have occupancies of 0.15 and 0.36 electrons in the case of (H$_2$O)$_4^-$, and 0.20 and 0.27 in (H$_2$O)$_6^-$. Second, there is a Ry NBO associated with the ghost atom [Figure 3e], representing the most diffuse bit of the density and possessing an occupancy of 0.13 in (H$_2$O)$_4^-$ and 0.10 in (H$_2$O)$_6^-$. Together, these three NBOs represent that part of the unpaired electron distribution that does not penetrate into the water network.

Last there are the two σ_{OH}^* NBOs on the AA water molecule, which possess occupancies ranging from 0.10 to 0.16 electrons at the B3LYP level, comparable to the σ_{OH}^* occupancies in the strongly H-bonded fluoride, oxide, and hydroxide monohydrates. Whereas the large σ_{OH}^* occupancies in these X$^-$(H$_2$O) complexes manifest as vibrational red-shifts of 2100−3000 (ref 19), in the case of AA isomers of (H$_2$O)$_n^-$ the red-shift is "only" 300 cm^{-1}. This is closer to the 570 cm^{-1} shift observed for Cl$^-$(H$_2$O), which has a σ_{OH}^* occupancy of 0.036, far smaller than the AA σ_{OH}^* occupancies. This disparity seems even more stark when one considers that the σ_{OH}^* occupancies for

(43) Shin, J.-W.; Hammer, N. I.; Headrick, J. M.; Johnson, M. A. *Chem. Phys. Lett.* **2004**, *399*, 349.
(44) Xantheas, S. S.; Burnham, C. J.; Harrison, R. J. *J. Chem. Phys.* **2002**, *116*, 1493.
(45) James, T.; Wales, D. J.; Hernández-Rojas, J. *Chem. Phys. Lett.* **2005**, *415*, 302.
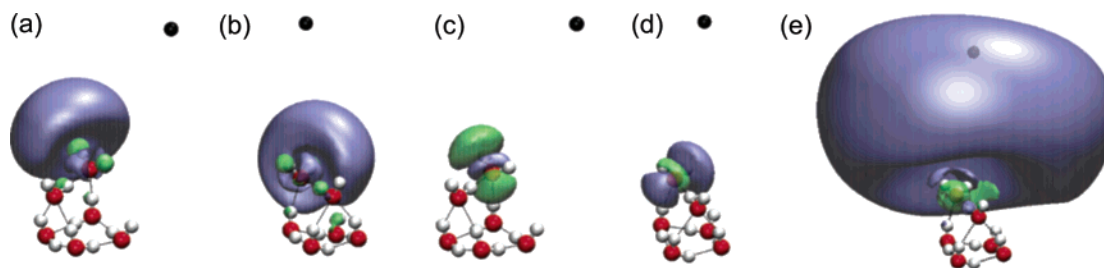
Figure 3. B3LYP NBOs associated with the excess electron for AA $(H_2O)_6^-$. Orbitals (a) and (b) are Ry_H^* NBOs with occupancies of 0.20 and 0.27, respectively; (c) and (d) are σ_{OH}^* NBOs with occupancies of 0.12 and 0.15, respectively; and (e) is a Ry_H^* NBO with an occupancy of 0.10. Orbitals (a−d) are plotted using a contour value of 0.020 au, while (e) is significantly more diffuse and is plotted using a contour value of 0.005 au. Black spheres represent the ghost atom.

Table 2. NBO Donor−Acceptor (D → A) Stabilization Energies for the AA Isomer of $(H_2O)_6^-$

D → A interaction	$\Delta E_{D \to A}$ (kcal/mol)[a]		D → A interaction	$\Delta E_{D \to A}$ (kcal/mol)[a]	
	HF[b]	B3LYP[b]		HF[b]	B3LYP[b]
$n(O_{13}) \to \sigma^*(O_{10}H_{12})$	26.9	23.2	$Ry(H_3) \to \sigma_{OH}^*(O_1H_3)$	−	23.2
$n(O_1) \to \sigma^*(O_4H_6)$	21.0	18.5	$Ry(H_3) \to Ry^*(H_{14})$	−	7.8
$n(O_{10}) \to \sigma^*(O_7H_9)$	18.6	16.4	$Ry(H_3) \to Ry^*(H_3)$	−	5.3
$n(O_{16}) \to \sigma^*(O_{13}H_{15})$	18.8	16.4	$Ry(H_3) \to \sigma^*(O_1H_2)$	−	5.0
$n(O_7) \to \sigma^*(O_{16}H_{18})$	16.7	15.0	$Ry(H_2) \to Ry^*(H_2)$	−	4.4
$n(O_1) \to \sigma^*(O_{13}H_{14})$	10.0	9.8	$Ry(Gh) \to Ry^*(H_3)$	6.7	−
$n(O_4) \to \sigma^*(O_7H_8)$	8.7	8.3	$Rh(Gh) \to Ry^*(H_2)$	4.1	−
$n(O_4) \to \sigma^*(O_{16}H_{17})$	4.5	8.4		−	−

[a] All stabilization energies larger than 4.0 kcal/mol per electron are listed. [b] 6-31++G*-f(2+) basis at the B3LYP/6-31++G*-f(2+) geometry.

Table 3. NBO σ_{OH}^* Occupancies for the AA Isomer of $(H_2O)_6^-$

σ_{OH}^* orbital	HF[a]		MP2[a]		B3LYP[a]	
	α	β	α	β	α	β
O_1-H_2	0.022	0.000	0.072	0.010	0.117	0.001
O_1-H_3	0.026	0.000	0.090	0.010	0.147	0.001
O_4-H_5	0.001	0.000	0.013	0.011	0.013	0.001
O_4-H_6	0.014	0.013	0.031	0.027	0.036	0.020
O_7-H_8	0.006	0.006	0.017	0.017	0.010	0.009
O_7-H_9	0.012	0.012	0.025	0.025	0.018	0.017
$O_{10}-H_{11}$	0.000	0.000	0.011	0.010	0.006	0.000
$O_{10}-H_{12}$	0.018	0.018	0.032	0.032	0.026	0.026
$O_{13}-H_{14}$	0.006	0.006	0.019	0.018	0.014	0.010
$O_{13}-H_{15}$	0.013	0.013	0.026	0.026	0.019	0.019
$O_{16}-H_{17}$	0.003	0.003	0.014	0.014	0.006	0.005
$O_{16}-H_{18}$	0.012	0.012	0.026	0.025	0.018	0.018

[a] 6-31++G*-f(2+) basis at the B3LYP geometry.

$X^-(H_2O)$ listed in Table 1 represent sums of α- and β-spin contributions (since the donor orbital is a lone pair), whereas for $(H_2O)_n^-$ the σ_{OH}^* occupancies arise almost entirely from the α space. This apparent paradox—that comparable σ_{OH}^* occupancies in $(H_2O)_n^-$ and $X^-(H_2O)$ engender vastly disparate vibrational red-shifts—is resolved later in this work.

Electron Correlation and Charge Penetration. Having suggested large σ_{OH}^* occupancies as the origin of the vibrational red-shifts in AA $(H_2O)_n^-$, we next identify the origin of these large occupancies by examining donor−acceptor stabilization interactions. Table 2 lists the significant donor−acceptor interactions for the AA isomer of $(H_2O)_6^-$ at both the HF and the B3LYP level. (The AA tetramer anion exhibits a similar set of orbital interactions.) These interactions fall into two categories, the first being the $n_O \to \sigma_{OH}^*$ charge-transfer associated with water−water H-bonds. As with the H-bond in $X^-(H_2O)$, the $n \to \sigma_{OH}^*$ interaction energy is large even in the absence of electron correlation, as a result of mean-field induction that polarizes the electron density along the H-bond axis.[46,47]

The second set of orbital interactions, involving the unpaired electron, changes qualitatively upon incorporation of electron correlation. At the B3LYP level, these interactions involve donation from Ry NBOs on AA hydrogen atoms (e.g., Figure 3a,b) into other, weakly occupied Ry orbitals situated on these and other dangling hydrogen atoms, and also into σ_{OH}^* orbitals. Just as in $X^-(H_2O)$, where a single $n_X \to \sigma_{OH}^*$ stabilization energy dominates the donor−acceptor interactions, the AA hydrated-electron isomers exhibit a single large $e^- \to \sigma_{OH}^*$ interaction, comparable to or larger than any of the interactions associated with water−water H-bonds. At the MP2 level, this

(46) Reed, A. E.; Weinhold, F. *J. Chem. Phys.* **1983**, *78*, 4066.
(47) Reed, A. E.; Weinhold, F.; Curtiss, L. A.; Pochatko, D. J. *J. Chem. Phys.* **1986**, *84*, 5687.

stabilization energy is only half as large as the B3LYP value, but the $e^- \to \sigma_{OH}^*$ charge-transfer mechanism still stands out as the only significant orbital interaction aside from those associated with water−water H-bonding.

The excess-electron orbital interactions are quite different at the HF level, reflecting a very different structure of the excess-electron NBOs. The HF NBOs are less tightly bound to the water network and consequently are classified as ghost-atom Ry orbitals or H−Gh σ bonds. These NBOs exhibit a small number of delocalizing interactions with other orbitals of this type, but the interaction energies are much smaller than the $e^- \to \sigma_{OH}^*$ interaction obtained at correlated levels of theory. Moreover, if we use a HF-optimized geometry (as opposed to the B3LYP geometries used in Table 2), orbital interactions associated with the unpaired electron vanish completely at the HF level, and one obtains a single excess-electron NBO with an occupancy greater than 0.9. This NBO is localized at the positive end of the cluster dipole moment vector, consistent with purely electrostatic binding of the excess electron. The same behavior at the HF level was also documented in a much earlier NBO analysis of water cluster anions.[48]

A more incisive measure of the effect of electron correlation comes from the σ_{OH}^* NBO occupancies, which are listed in Table 3 for each O−H bond of the AA isomer of $(H_2O)_6^-$. [Values for AA $(H_2O)_4^-$ are similar.] At the HF level, water−water H-bonds are characterized by a transfer of 0.01−0.03 electrons into the σ_{OH}^* orbital of the hydrogen donor (typical of H-bonds between neutral molecules[33,46,47]), and electron correlation increases these σ_{OH}^* occupancies to 0.02−0.04 electrons. Meanwhile, σ_{OH}^* occupancies on the AA water molecule

(48) Reed, A. E.; Clark, T. *Faraday Discuss. Chem. Soc.* **1988**, *85*, 365.

Table 4. NBO Donor−Acceptor Stabilization Energies for the Book Isomers of $(H_2O)_6^-$ and $(H_2O)_6$

	$\Delta E_{D \rightarrow A}$ (kcal/mol)[a]			
	HF[b]		B3LYP[b]	
donor-acceptor interaction	neutral	anion	neutral	anion
$n(O_1) \rightarrow \sigma^*(O_{16}H_{18})$	34.0	34.4	28.7	29.4
$n(O_7) \rightarrow \sigma^*(O_4H_6)$	33.4	26.5	28.2	22.6
$n(O_4) \rightarrow \sigma^*(O_1H_3)$	29.8	25.1	25.4	21.7
$n(O_{13}) \rightarrow \sigma^*(O_{10}H_{12})$	21.9	22.5	18.9	19.9
$n(O_{10}) \rightarrow \sigma^*(O_7H_9)$	20.6	19.8	18.0	18.7
$n(O_{16}) \rightarrow \sigma^*(O_{13}H_{15})$	18.6	17.3	16.4	15.7
$n(O_{16}) \rightarrow \sigma^*(O_7H_8)$	10.6	10.7	10.1	10.2
$Ry(H_2) \rightarrow \sigma^*(O_1H_2)$	−	−	−	5.3
$Ry(H_2) \rightarrow \sigma^*(O_1H_3)$	−	−	−	2.3
$Ry(H_2) \rightarrow Ry^*(H_3)$	−	−	−	4.1
$n(Gh) \rightarrow Ry^*(H_{14})$	−	2.1	−	−

[a] All stabilization energies larger than 2.0 kcal/mol per electron (4.0 kcal/mol, for the spin-paired $n \rightarrow \sigma^*_{OH}$ H-bond interactions) are listed. [b] 6-31++G*-f(2+) basis at the B3LYP geometry.

$(H_2-O_1-H_3)$ increase from around 0.02−0.03 at the HF level to 0.12−0.15 in a B3LYP calculation, comparable to the σ^*_{OH} occupancy in $F^-(H_2O)$. The AA σ^*_{OH} occupancies are somewhat smaller at the MP2 level, but still significantly larger than those associated with water−water H-bonds.

Importantly, the $\sigma^*_{OH}(AA)$ occupancies arise essentially entirely from α-spin electrons, which unambiguously identifies these occupancies as manifestations of $e^- \rightarrow \sigma^*_{OH}$ penetration. A small amount of spin polarization is also observed in the dangling O−H bonds on water molecules adjacent to the AA water [e.g., O_4-H_5 in $(H_2O)_4^-$ and $(H_2O)_6^-$], but beyond this "second solvation shell" there is no spin polarization and hence no penetration of the unpaired electron. There is also little or no penetration into the σ^*_{OH} orbitals associated with water− water H-bonds.

Thus far we have confined our analysis of $(H_2O)_n^-$ mainly to AA-type isomers. These are prominent in both vibrational and photoelectron spectra,[2−5,7,43] but they are not the only isomers present in these spectra.[3,6,43] We next discuss NBO analysis of cyclic $(H_2O)_4^-$ [Figure 1b] and the book isomer of $(H_2O)_6^-$ [Figure 2b]. Unlike the AA-type water networks, which are very high in energy on the neutral cluster potential surface,[6,49,50] the cyclic- and book-type networks are closely related to stable structures on the neutral cluster potential surfaces. We will compare cyclic $(H_2O)_4^-$ to the $(H_2O)_4$ global minimum,[44,45] Figure 1c, and the book-like isomer of $(H_2O)_6^-$ to a similar book-like isomer of $(H_2O)_6$ that lies only slightly above the global minimum for the neutral hexamer.[44]

Table 4 lists the significant donor−acceptor stabilization energies for the book isomer of $(H_2O)_6^-$, with cyclic $(H_2O)_4^-$ affording a similar story. The only significant stabilization energies are $n \rightarrow \sigma^*_{OH}$ interactions whose values are typical of water−water H-bonds. Donation from the unpaired electron does not induce any large stabilization energies.

Occupancies of the σ^*_{OH} NBOs for book-type $(H_2O)_6$ and $(H_2O)_6^-$ are listed in Table 5. The anion binds the extra electron via four dangling hydrogen atoms, and $e^- \rightarrow \sigma^*_{OH}$ charge transfer is once again evident in the spin-polarized nature of the σ^*_{OH} occupancies corresponding to dangling O−H

(49) Smith, D. M. A.; Smets, J.; Elkadi, Y.; Adamowicz, L. *J. Chem. Phys.* **1998**, *109*, 1238.
(50) Kim, J.; Suh, S. B.; Kim, K. S. *J. Chem. Phys.* **1999**, *111*, 10077.

Table 5. NBO σ^*_{OH} Occupancies for the Book Isomers of $(H_2O)_6^-$ and $(H_2O)_6$

	HF[a]			MP2[a]			B3LYP[a]		
	neutral	anion		neutral	anion		neutral	anion	
σ^*_{OH} orbital	α	α	β	α	α	β	α	α	β
O_1-H_2	0.000	0.003	0.000	0.010	0.018	0.010	0.000	0.037	0.000
O_1-H_3	0.018	0.016	0.016	0.032	0.031	0.031	0.026	0.031	0.023
O_4-H_5	0.000	0.001	0.000	0.010	0.013	0.010	0.000	0.018	0.000
O_4-H_6	0.021	0.018	0.017	0.036	0.032	0.032	0.029	0.027	0.025
O_7-H_8	0.007	0.007	0.007	0.019	0.019	0.019	0.010	0.012	0.010
O_7-H_9	0.013	0.012	0.013	0.026	0.026	0.026	0.019	0.020	0.019
$O_{10}-H_{11}$	0.000	0.001	0.000	0.010	0.013	0.010	0.000	0.017	0.000
$O_{10}-H_{12}$	0.013	0.014	0.014	0.026	0.028	0.028	0.019	0.026	0.021
$O_{13}-H_{14}$	0.000	0.002	0.000	0.010	0.017	0.010	0.000	0.032	0.000
$O_{13}-H_{15}$	0.012	0.011	0.011	0.024	0.025	0.025	0.017	0.025	0.016
$O_{16}-H_{17}$	0.000	0.001	0.000	0.010	0.011	0.011	0.001	0.012	0.001
$O_{16}-H_{18}$	0.021	0.022	0.022	0.036	0.038	0.038	0.029	0.038	0.031

[a] 6-31++G*-f(2+) basis at the B3LYP geometry.

bonds. These occupancies, however, are significantly smaller than those observed for the AA σ^*_{OH} orbitals in AA-type isomers, less than 0.04 in all cases, and thus more comparable to water−water H-bonds than to the AA σ^*_{OH} antibonds. This is consistent with the smaller VEBEs and increased dipole-bound character of the SOMO in cyclic $(H_2O)_4^-$ and book-type $(H_2O)_6^-$, as compared to the AA isomers.[3,35] The former do not exhibit nearly the same degree of e^- penetration, and what little penetration exists is essentially absent at the HF level.

Detailed Analysis of Vibrational Spectra. We next analyze vibrational spectra for all of the neutral and anionic water cluster isomers introduced above. Spectra are obtained from scaled harmonic frequencies, as discussed in Computational Methods, and frequencies quoted in the text include this scaling. We omit any discussion of deuterated clusters since $(H_2O)_n^-$ is the more interesting isotopologue, and because there is no compelling computational reason to deuterate the clusters. (Experimentally, deuteration is necessary when $v = 1$ of the anion lies above the electron detachment threshold.) Indeed, one advantage of our computational study is that we may consider the vibrational spectrum of a cluster-like cyclic $(H_2O)_4^-$, whose VEBE is only 0.06 eV (480 cm^{-1}). Since the D−O−D bend fundamental is approximately 1200 cm^{-1}, there is no chance of measuring an experimental vibrational spectrum for this isomer in isolation. Nevertheless, the computed spectrum offers an interesting comparison to that of AA $(H_2O)_4^-$.

The major conclusions reached above—that vibrational red-shifts in $(H_2O)_n^-$ arise from $e^- \rightarrow \sigma^*_{OH}$ charge transfer and that this effect is due almost entirely to electron correlation— are borne out by comparison of the vibrational spectra for $(H_2O)_4^-$ and $(H_2O)_4$ in Figure 4. The free O−H stretching frequencies are quite similar in the anionic and neutral clusters isomers, indicating no appreciable e^- penetration into the non-AA water molecules. Scaled HF and B3LYP frequencies for the free O−H stretches also agree quite well, implying that neither electron correlation effects nor anharmonicity are radically different for the free O−H modes than they are in isolated H_2O. This further suggests that there is little e^- penetration into non-AA water molecules.

The situation is quite different for the O−H stretch vibrations of the AA water molecule. At the HF level, the AA symmetric and asymmetric stretching modes appear as intense transitions located at 3594 and 3692 cm^{-1}, respectively (see Figure 4a),
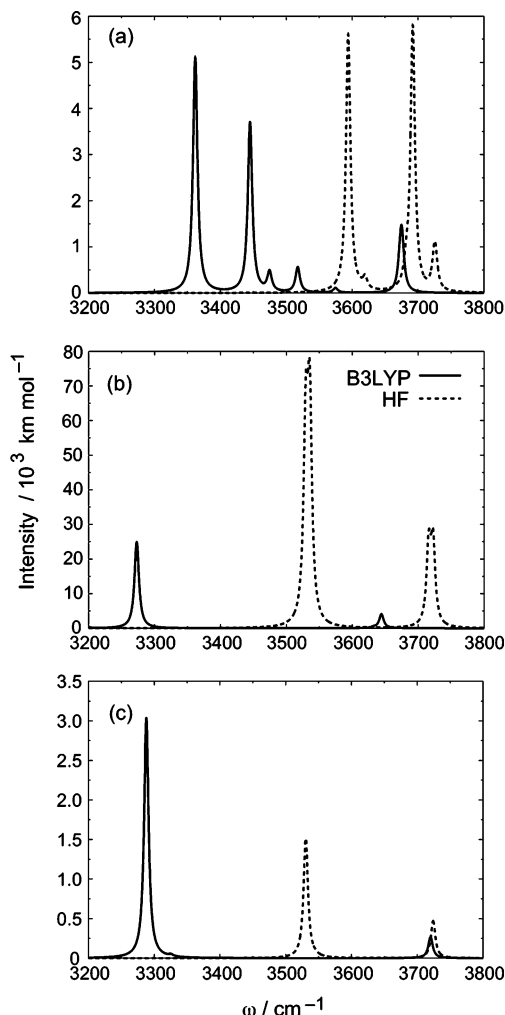
Figure 4. B3LYP and HF vibrational spectra in the O−H stretching region for (a) the AA isomer of $(H_2O)_4^-$, (b) the cyclic isomer of $(H_2O)_4^-$, and (c) the cyclic isomer of $(H_2O)_4$. Each panel uses a different intensity scale.

corresponding to red-shifts of $\delta\omega = -131$ cm^{-1} and $\delta\omega = -33$ cm^{-1} relative to the free O−H stretch. The enhanced intensities are consistent with large changes in the local electrostatics around the AA water molecule, with concomitant "charge sloshing" upon vibrational excitation. HF theory does predict a sizable red-shift for the AA symmetric stretch vibration, but this largely reflects the fact that the normal mode in question contains a significant component of H-bonded proton stretching motions. Indeed, the nominal H-bonded proton stretching vibrations appear as a high-frequency, low-intensity shoulder to the AA symmetric stretch peak in Figure 4a. In contrast to the symmetric stretch, the AA asymmetric stretching mode is localized entirely on the AA water molecule, and its frequency is only slightly red-shifted at the HF level.

Red-shifts obtained at the B3LYP level are much larger (and also consistent with experiment[6]): $\delta\omega = -313$ cm^{-1} and $\delta\omega = -230$ cm^{-1} for the AA symmetric and asymmetric stretch vibrations, respectively. The H-bonded proton-stretching modes, which appear as a pair of weak transitions around 3500 cm^{-1} ($\delta\omega < 200$ cm^{-1}), are separated from the AA peaks, in contrast to the HF result. Thus, the frequency shift of the AA modes is almost entirely an electron correlation effect, consistent with our explanation of this red-shift as correlation-induced $e^- \rightarrow \sigma_{OH}^*$ charge transfer.
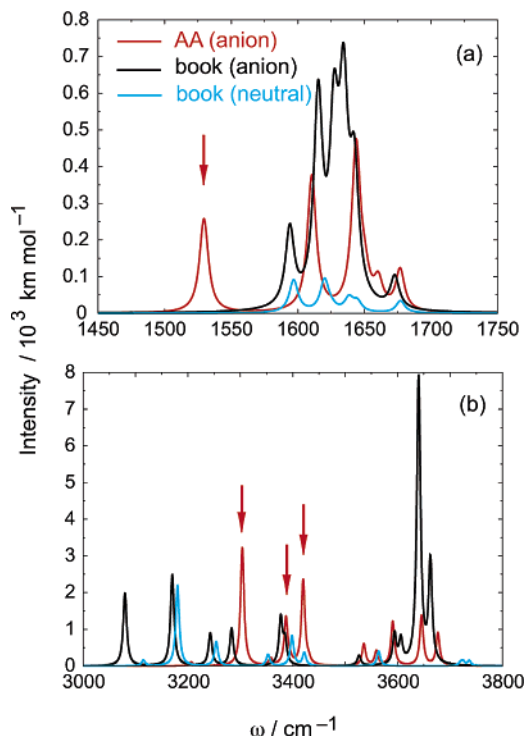

Figure 5. B3LYP vibrational spectra in (a) the H−O−H bending region and (b) the O−H stretching region, for isomers of $(H_2O)_6$ and $(H_2O)_6^-$. Arrows indicate normal modes with significant contributions from the AA water molecule.

The vibrational spectrum of cyclic $(H_2O)_4^-$ is shown in Figure 4b, and at the HF level its most intense feature is the H-bonded proton stretching band at 3532 cm^{-1} ($\delta\omega = -187$ cm^{-1}). This is about the same red-shift as noted above, at the HF level, for the H-bonded stretches in the AA isomer. B3LYP places this same band at 3273 cm^{-1}, for a much more substantial red-shift of $\delta\omega = -371$ cm^{-1}, but upon comparison to the vibrational spectrum of the neutral tetramer (Figure 4c), we discover that this shift is not due to the extra electron at all, but arises solely from H-bonding. The extra electron in cyclic $(H_2O)_4^-$ instead manifests as a shift of -77 cm^{-1} in the free O−H frequency, relative to its value in the neutral tetramer, indicating a very small amount of charge transfer into the dangling O−H antibonds. The extra electron does leave a significant mark on the infrared intensities, however, as seen from the vastly different intensities in b versus c of Figure 4.

B3LYP vibrational spectra for $(H_2O)_6$, and for both isomers of $(H_2O)_6^-$, are shown in Figure 5. It is known, both from experiments[51] and from electronic structure calculations,[52−56] that all of the bending frequencies in neutral water clusters are blue-shifted relative to the 1595 cm^{-1} bend in isolated H_2O, and we find that this is also the case in non-AA isomers of $(H_2O)_n^-$. For the AA isomers, the bends associated with non-AA water molecules are blue-shifted, but the AA bend is red-shifted relative to isolated H_2O (see Figure 5a). In the stretching spectrum of the AA isomer (Figure 5b), three vibra-

(51) Paul, J. B.; Provencal, A.; Chapo, C.; Roth, K.; Casaes, R.; Saykally, R. J. *J. Phys. Chem. A* **1999**, *103*, 2972.
(52) Xantheas, S. S.; Dunning, T. H., Jr. *J. Chem. Phys.* **1993**, *99*, 8774.
(53) Xantheas, S. S. *J. Chem. Phys.* **1995**, *102*, 4505.
(54) Kim, J.; Kim, K. S. *J. Chem. Phys.* **1998**, *109*, 5886.
(55) van der Rest, G.; Masella, M. *J. Mol. Spectrosc.* **1999**, *196*, 146.
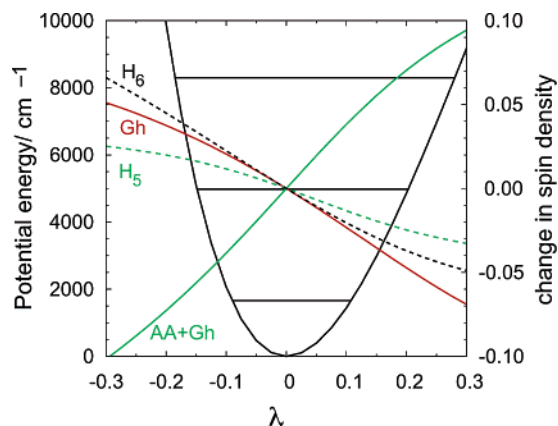(56) Sadlej, J. *Int. J. Quantum Chem.* **2002**, *90*, 1191.

Figure 6. Potential energy and changes in atomic NSDs in $(H_2O)_6^-$ along the AA symmetric stretch normal mode. The abscissa λ represents a scalar multiple of the Cartesian displacements that define the normal coordinates at equilibrium. Calculations were performed at the B3LYP/6-31++G*-f(2+) level, and vibrational energy levels represent harmonic estimates.

tional modes contain significant contributions from the AA water molecule and exhibit shifts of $\delta\omega = -257, -290$, and -373 cm^{-1} relative to the free O—H stretch (O$_{10}$—H$_{11}$ in Figure 2a). Although these are the most red-shifted frequencies in the vibrational spectrum of AA $(H_2O)_6^-$, both the book isomer of $(H_2O)_6^-$ and the book isomer of $(H_2O)_6$ exhibit H-bonded proton stretching modes at even lower frequencies. Thus, the bending region of the spectrum proves to be a better fingerprint of the AA binding motif than does the O—H stretching region.

Vibrational Excitation and the Difference between $(H_2O)_n^-$ and $X^-(H_2O)$. We have shown above that charge penetration beyond the AA water is not significant at the cluster's equilibrium geometry. Here we consider whether this remains the case following excitation of the AA vibrational modes, which (as indicated by their large infrared intensities) are associated with substantial changes in the SOMO. The AA isomer of $(H_2O)_6^-$ is especially interesting in this regard, because both its AA symmetric and asymmetric stretching modes contain significant components of the O$_4$—H$_6$ stretch (see Figure 2a). It has been speculated that this coupling might drive charge transfer into a second, DAA-type water molecule.[2]

To investigate whether this is in fact the case, we examine a one-dimensional potential along the AA symmetric stretch normal mode, calculated at the B3LYP/6-31++G*-f(2+) level and plotted in Figure 6. This figure also tracks the changes in selected atomic natural spin densities (NSDs) along this coordinate. The NSDs are defined as the difference between α and β natural populations[33,34,57] on a given atom, and provide an atomic partition of the unpaired electron.

At the equilibrium geometry of the cluster, the sum of the NSDs on the ghost atom and the AA water molecule is 0.85, meaning that 15% of the total spin density has penetrated beyond the AA water molecule. Of this, 12% is distributed over the aforementioned DAA water molecule (H$_5$—O$_4$—H$_6$), and the rest is located on H$_{12}$. The sum of the AA and ghost-atom NSDs fluctuates between 0.82 and 0.89 in the vibrational ground state (as delineated by the classical turning points) and varies from 0.80 to 0.90 in $\upsilon = 1$ of the symmetric stretch, a minute change that indicates vibrational excitation does not promote e^-
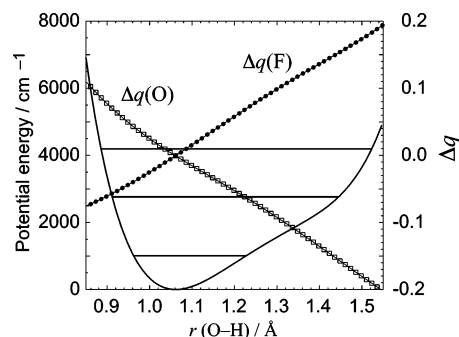
(57) Reed, A. E.; Weinstock, R. B.; Weinhold, F. *J. Chem. Phys.* **1985**, *83*, 735.

Figure 7. F$^-$(H$_2$O) potential energy curve for the shared proton coordinate, along with the changes in natural atomic charges on the O and F atoms. Calculations were performed at the B3LYP/6-31++G* level using a grid spacing of 0.0125 Å. Vibrational energy levels at 1004, 2764, and 4192 cm^{-1} were obtained by fitting to a Morse potential.
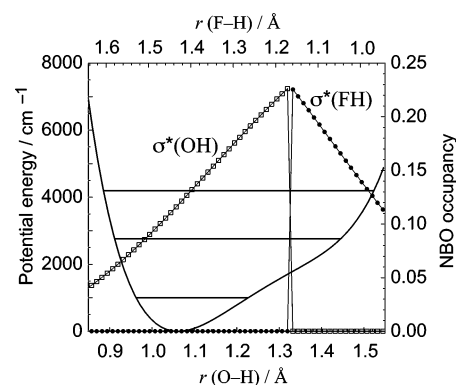

Figure 8. F$^-$(H$_2$O) potential energy curve for the shared proton coordinate, along with the occupancies of the σ_{OH}^* and σ_{FH}^* NBOs.

penetration. Excitation of the AA asymmetric stretch also does not facilitate additional charge penetration.

To put this in perspective, we next examine a one-dimensional B3LYP/6-31++G* potential for F$^-$(H$_2$O) along the shared-proton coordinate.[58] We choose this system because it exhibits σ_{OH}^* occupancies at the B3LYP level that are similar to those obtained for the σ_{OH}^*(AA) orbitals. However, unlike the AA stretching potential in Figure 6, which is fairly harmonic, the shared-proton stretching potential in F$^-$(H$_2$O) exhibits a characteristic "shelf" structure,[19,20,24] as shown in Figure 7. This anharmonicity significantly reduces the energy in $\upsilon = 1$, relative to an harmonic estimate, and is thus the proximate cause of the large red-shift in the shared-proton stretching frequency.

Since atomic NSDs are zero for this closed-shell system, we instead examine natural charges on the F and O atoms. The changes in these quantities, relative to their values at the equilibrium geometry, are plotted along with the B3LYP potential in Figure 7. The natural charges fluctuate by ± 0.06 in the vibrational ground state, but upon $\upsilon = 0 \rightarrow 1$ excitation the shared proton can shuttle as much as 0.2 electrons from F to O, a much more substantial charge transfer than is possible even in $\upsilon = 2$ of the AA stretching modes in $(H_2O)_6^-$.

This charge-transfer capability is reflected in the occupancies of the σ_{OH}^* and σ_{FH}^* NBOs, which are plotted in Figure 8. Each of these occupancies exhibits a discontinuity at $r_{OH} = 1.32825$ Å ($r_{FH} = 1.15732$ Å). The occupancies of the σ_{OH} and σ_{FH}

(58) For convenience we use a collinear F—H—O geometry, as the equilibrium bond angle is 174° and the optimized collinear structure lies only 141 cm^{-1} above the global minimum.

bonding orbitals exhibit discontinuities at the same location, where they abruptly switch from ~1.998 electrons to zero. (Each of these discontinuities remains abrupt even when the grid spacing is reduced to 0.0001 Å.) The same type of discontinuity has been documented previously, in the context of intramolecular proton transfer, by Pacios et al.,[59] who discuss this phenomena in terms of an instantaneous charge transfer of a fraction of an electron occurring at a particular value of the donor−acceptor separation. Note, however, that the natural charges in Figure 7 evolve continuously, and there is no abrupt "hopping" of an electron from one moiety to another. Rather, the discontinuity in the NBO occupancies signals an abrupt change in the optimal description of the bonding, or in other words, a crossing of diabatic potentials. One of these corresponds to F$^-$···HOH and the other to FH···$^-$OH.

Importantly, this crossing occurs at a value of r_{OH} that is beyond the classical turning point in $v = 0$ but accessible in $v = 1$. Thus, one way to understand the enormous red-shift of the shared proton stretch in F$^-$(H$_2$O) is that vibrational excitation renders a second diabatic state energetically accessible, thereby facilitating a vibrationally driven change in electron configuration. The intersection of the two diabats manifests as extreme anharmonicity in the adiabatic potential that substantially lowers the $v = 0 \rightarrow 1$ excitation energy. There is no evidence that such a mechanism is available to the (H$_2$O)$_n^-$ clusters studied here, for which the H + $^-$OH(H$_2$O)$_{n-1}$ diabat is apparently too high in energy to influence the ground-state adiabatic potential. Consequently, the ionic vibrational modes in (H$_2$O)$_n^-$ are much more harmonic than those of F$^-$(H$_2$O). Thus, while the degree of charge penetration into the water network may be just as large in AA-type (H$_2$O)$_n^-$ clusters as it is in certain X$^-$(H$_2$O) systems, vibrational red-shifts are much smaller in the former case, owing to the lack of a sufficiently strong base that can induce a second low-energy diabatic state.

Conclusions and Implications

We have shown that the electronic structure of small hydrated-electron clusters can be conceptualized in terms of a small number of partially occupied "excess-electron" NBOs localized around the dangling hydrogen atoms that support the SOMO. For isomers exhibiting the AA electron binding motif, these partially occupied NBOs notably include σ_{OH}^* orbitals on the AA water molecule, whose occupancies range from 0.10 to 0.16 electrons in the examples considered here. Penetration of the electron into σ_{OH}^* orbitals, which is almost entirely an electron correlation effect, gives rise to intense infrared transitions that are red-shifted by about 300 cm^{-1} relative to the free O−H stretch. This novel mechanistic assignment for the red-shift is corroborated by the much smaller red-shifts calculated for

isomers such as cyclic (H$_2$O)$_4^-$, where $e^- \rightarrow \sigma_{OH}^*$ penetration is greatly diminished. Although the vibrational spectrum of cyclic (H$_2$O)$_4^-$ cannot be obtained experimentally (owing to vibrationally induced autodetachment), (H$_2$O)$_n^-$ clusters in the $n = 20-24$ régime exhibit surface-bound, non-AA isomers with large VEBEs,[35,36] whose vibrational spectra could in principle be obtained experimentally.

The $e^- \rightarrow \sigma^*$ "penetration" documented in this work should not be confused with "leakage" (delocalization) of the SOMO into the interstices between water molecules, of the sort observed in Car−Parrinello simulations of the aqueous electron.[60] The two phenomena are distinct (although not mutually exclusive), and the distinction has a direct bearing on the design of electron−water pseudopotentials for quantum/classical simulations of the hydrated electron. Delocalization is possible even with only a single quantum−mechanical electron and a purely electrostatic electron−water pseudopotential,[61,62] but the $e^- \rightarrow \sigma_{OH}^*$ penetration described in this work is a many-electron phenomenon. Whether this phenomenon is captured by the Drude-type electron−water Hamiltonians developed recently by Wang and Jordan,[63,64] which include an additional quantum−mechanical degree of freedom on each water molecule, is an open question.

Our analysis reveals that the extent of $e^- \rightarrow \sigma_{OH}^*$ charge transfer can be comparable to the $n \rightarrow \sigma_{OH}^*$ charge transfer in strongly H-bonded anion−water complexes, but hydrated-electron clusters are ultimately rather different from other X$^-$(H$_2$O)$_n$ systems. The existence of two low-energy diabatic states in X$^-$(H$_2$O), corresponding to X$^-$···HOH and XH···$^-$OH, gives rise to significant anharmonicity in the shared-proton vibrational modes that is not present in the ionic modes of (H$_2$O)$_n^-$, and which leads to significantly larger vibrational red-shifts in X$^-$(H$_2$O), despite comparable charge penetration into σ_{OH}^* orbitals.

Supporting Information Available: Complete citation for ref 39. This material is available free of charge via the Internet at http://pubs.acs.org.

JA064949I

(59) Pacios, L. F.; Gálvez, O.; Gómez, P. C. *J. Chem. Phys.* **2005**, *122*, 214307.

(60) Boero, M.; Parrinello, M.; Terakura, K.; Ikeshoji, T.; Liew, C. C. *Phys. Rev. Lett.* **2003**, *90*, 226403.
(61) Barnett, R. N.; Landman, U.; Cleveland, C. L.; Jortner, J. *J. Chem. Phys.* **1988**, *88*, 4429.
(62) Turi, L.; Sheu, W.-S.; Rossky, P. J. *Science* **2005**, *309*, 914.
(63) Wang, F.; Jordan, K. D. *J. Chem. Phys.* **2001**, *114*, 10717.
(64) Wang, F.; Jordan, K. D. *J. Chem. Phys.* **2002**, *116*, 6973.